Space Frequency Coordination Group

Report SFCG 38-1R1

POTENTIAL RFI TO EESS (ACTIVE) CLOUD PROFILE RADARS IN THE 94.0-94.1 GHZ FREQUENCY BAND AND EESS (PASSIVE) RADIOMETERS IN THE 86-92 GHZ FREQUENCY BAND FROM OTHER SERVICES

Abstract

This new SFCG report analyzes potential RFI into EESS (active) cloud profile radar systems operating in the 94.0-94.1 GHz frequency band and EESS (passive) radiometers operating in the 86-92 GHz frequency band from systems in other services. Included in the report are the characteristics of the EESS (active) and EESS (passive) systems, the characteristics of systems in other services, and RFI analyses of potential RFI into the EESS (active) systems from systems in other services near 94 GHz and potential RFI into the EESS (passive) systems from systems in other services near 86-92 GHz.

Table of Contents

1. Introduction

The 94.0-94.1 GHz band is allocated to Earth Exploration-Satellite Service (EESS) (active) on a primary basis for EESS (active) spaceborne active sensors, such as cloud profile radars (CPRs). Herein are presented technical characteristics of two typical EESS (active) cloud profile radar systems operating in the frequency band 94.0-94.1 GHz and technical characteristics for systems into two other services: 1) typical Railway Radiocommunication Systems between Train and Trackside (RSTT) stations proposed for adjacent bands 92.0-94.0 GHz and 94.1-96.0 GHz and 2) typical FOD detection systems proposed for bands 92.0-100.0 GHz. Performance criteria and interference criteria are provided for active spaceborne cloud profile radar operating in the 94.0-94.1 GHz frequency band. Preliminary calculations are performed to determine the amount of attenuation needed to be applied to railway RSTT systems out-of band (OOB) emission levels in relation to the RSTT in-band emission levels in order for the out-of-band RSTT emissions to not exceed the EESS (active) interference protection criteria levels and to determine the amount of attenuation needed to be applied to FOD detection systems in-band emission levels in order for the in-band FOD detection systems emissions to not exceed the EESS (active) interference protection criteria levels.

The 86-92 GHz band is allocated to Earth Exploration-Satellite Service (EESS) (passive) on a primary basis for EESS (passive) spaceborne passive sensors, such as radiometers. Herein are presented technical characteristics of a typical EESS (passive) radiometer system operating in the frequency band 86-92 GHz and technical characteristics for systems into two other services: 1) typical Railway Radiocommunication Systems between Train and Trackside (RSTT) stations proposed for adjacent band 92.0-94.0 GHz and 2) typical FOD detection systems proposed for bands 92.0-100.0 GHz. Performance criteria and interference criteria are provided for passive spaceborne radiometers operating in the 86-92 GHz frequency band. Preliminary calculations are performed to determine the amount of attenuation needed to be applied to railway RSTT systems out-of band (OOB) emission levels in relation to the RSTT in-band emission levels in order for the out-of-band RSTT emissions to not exceed the EESS (passive) interference protection criteria levels and to determine the amount of attenuation needed to be applied to FOD detection systems out-of-band emission levels in order for the out-of-band FOD detection systems emissions to not exceed the EESS (passive) interference protection criteria levels.

2. Characteristics of Earth exploration-satellite service (EESS) (active)

Technical characteristics of cloud profile radars (CPRs) in the frequency band of 94.0-94.1 GHz are given in Recommendation ITU-R RS.2105 – *Typical technical and operational characteristics of Earth exploration-satellite service (active) systems using allocations between 432 MHz and 238 GHz*. The technical characteristics for two CPR systems CPR-L1 and CPR-L2 are presented below in Table 1.

3. Performance and interference criteria of Earth exploration-satellite service (EESS) (active and passive)

Performance requirements for spaceborne active sensors in the EESS (active) are given in Recommendation ITU-R RS.1166-4 – *Performance and interference criteria for active spaceborne sensors*. The performance criteria for the EESS (active) cloud profile radars requires a measurement of a minimum reflectivity of –30 dBz ±10%, *I*/*N* no greater than –10 dB and random data availability criteria of no less than 95%.

Interference criteria for spaceborne active sensors in the EESS (active) are provided by Recommendation ITU-R RS.1166-4 – *Performance and interference criteria for active spaceborne sensors*. The interference threshold criteria for the EESS (active) Cloud Profile Radars in the 94.0-94.1 GHz frequency band is –155 dBW over 300 kHz.

Technical characteristics of spaceborne radiometers in the frequency band of 86-92 GHz including L-8 (which is considered the most sensitive) are provided in Recommendation ITU-R RS.1861 – *Typical technical and operational characteristics of Earth exploration-satellite service (passive) systems using allocations between 1.4 and 275 GHz*.

Performance requirements for spaceborne passive sensors in the EESS (passive) are provided by Recommendation ITU-R RS.2017 – *Performance and interference criteria for satellite passive remote sensing*. The performance criteria for the EESS (passive) radiometers specifies a temperature differential, ΔT_c of 0.05 K and data availability criteria of at least 99.99%.

TABLE 1

Characteristics of EESS (active) missions in the 94-94.1 GHz band

Parameter	CPR-L1	CPR-L2
Sensor type	Cloud Profiling Radar	Cloud Profiling Radar
Type of orbit	SSO	SSO
Altitude, km	705	393
Inclination, deg	98.2	97
Ascending Node LST	13:30	10:30[1]
Repeat period, days	16	25
Antenna type	Parabolic reflector to Offset Cassegrain antenna	Parabolic reflector
Antenna diameter	1.85-2.5 m	2.5 m
Antenna (transmit and receive) peak gain, dBi	63.1-65.2	65.2
Polarization	linear	LHC, RHC
Incidence angle at Earth, deg	0	0
Azimuth scan rate, rpm	0	0
Antenna beam look angle, deg	0	0
Antenna beam azimuth angle, deg	0	0
Antenna elev. beamwidth, deg	0.12	0.095
Antenna az. beamwidth, deg	0.12	0.095
Beam width, deg	0.095-0.108	0.095
RF Center Frequency, MHz	94.050	94.050
RF bandwidth, MHz	0.36	7
Transmit Pk pwr, W	1 000	1 430
Transmit Ave. pwr, W	21.31	28.8
Pulsewidth, µsec	3.33	3.3
Pulse Repetition Frequency (PRF), Hz	4 300	6 100-7 500
Chirp rate, MHz/µsec	N/A[2]	2.1

[1] Descending.

[2] The sensor uses an unmodulated pulse.

Parameter	CPR-L1	CPR-L2
Transmit duty cycle, %	1.33	2.01
Minimum sensitivity, dBz	–30 to –35	–30 to –35
Horizontal resolution	0.7-1.9 km	800 m
Vertical resolution	250-500 m	500 m
Doppler range	±10 m/s	–10 ~ +10 m/s
Doppler accuracy	1 m/s	1 m/s
System Noise Figure, dB	7	7

4. Compatibility studies for other services and (EESS) (active)

4.1 Compatibility studies for RSTT systems and (EESS) (active)

4.1.1 System architecture for RSTT systems

Figure 1 shows the schematic concept of the100 GHz wireless connection between on-board equipment and trackside radio access unit. The concept shows that 10 trackside radio access units with two antennas are equipped along the railway line. Two on-board transceivers are equipped with the driver's room located at the first car of the train and the conductor's room located at the end car of the train. Both on-board transceivers are complementally connected to the trackside radio access units to seamlessly maintain link connection through 100-GHz signals. If the space diversity is required to provide stable communication between train and trackside, the number of equipment becomes double.

FIGURE 1

Concept of 100-GHz wireless connection between on-board and trackside equipment

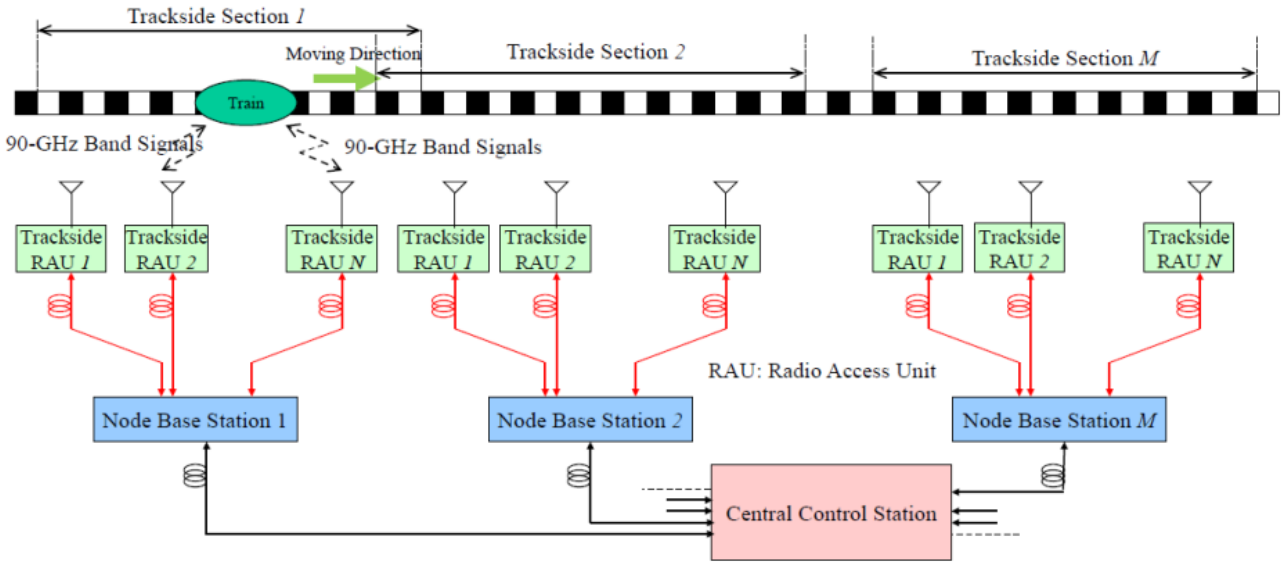

4.1.2 System characteristics for RSTT systems operating in bands 92-94 GHz, 94.1-100 GHz and 102-109.5 GHz

Table 2 summarizes technical and operational characteristics of RSTT stations operating in 92-94 GHz, 94.1-100 GHz and 102-109.5 GHz bands. The total bandwidth of 15.4 GHz can be used for data transmission between on-board radio equipment and trackside radio access units. The transmission distance of these equipment is designed by the railroad line environment.

TABLE 2

RSTT System parameters

Frequency range (GHz)	92-94. 94.1-100, 102-109.5
Seamless connection mechanism	Backward and forward switching method
Channel bandwidth (MHz)	400
Channelization (MHz)	See Figure 2
Channel aggregation pattern	See Figure 3
Antenna type	Cassegrain
Antenna gain (dBi)	44
Antenna beamwidth (degree)	1
Antenna height from rail surface (m)	4 (Maximum)
Polarization	Linear
Antenna pattern	See Figure 4
Average transmitting power (dBm)	10
Average e.i.r.p. (dBm)	54
Receiving noise figure (dB)	<10
Maximum transmission data rate (Gb/s)	5-10 (Stationary), 1 (Running)
Maximum transmission distance (km)	0.5-1 (Open), 3 (Tunnel)
Modulation	PSK, QPSK, 16QAM, 64QAM
Multiplexing method	FDD/TDD
Maximum running speed (km/h)	600
Wired interface of trackside radio access unit	[Recommendation ITU-T G.RoF]
Propagation model between train and trackside	Recommendation ITU-R P.1411

Figure 2 shows the channel arrangement of 100-GHz RSTT which is categorized into three groups. Each group has guard bands at both ends of frequency bands to avoid frequency interferences to the existing radiocommunication services. Figure 3 shows two channel aggregation pattern which is based on minimum Nyquist bandwidth of 250 MHz and roll-off rate of 0.35. This pattern can ideally transmit 1 Gb/s when QPSK modulation technique is used. Since the maximum data rate per channel is 2 Gb/s when 256 QAM modulation technique is applied, the 10 Gb/s data transmission is feasible by 4-channl aggregation pattern.

FIGURE 2

Channel arrangement of 100-GHz RSTT

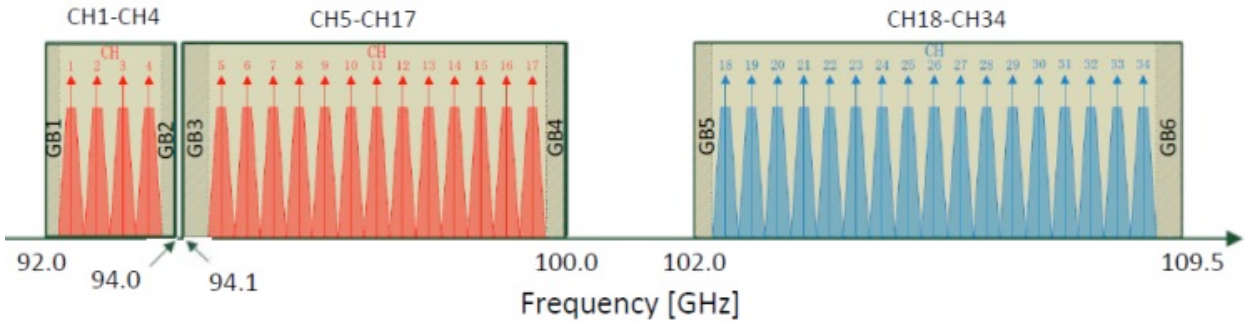

FIGURE 3

Channel aggregation pattern

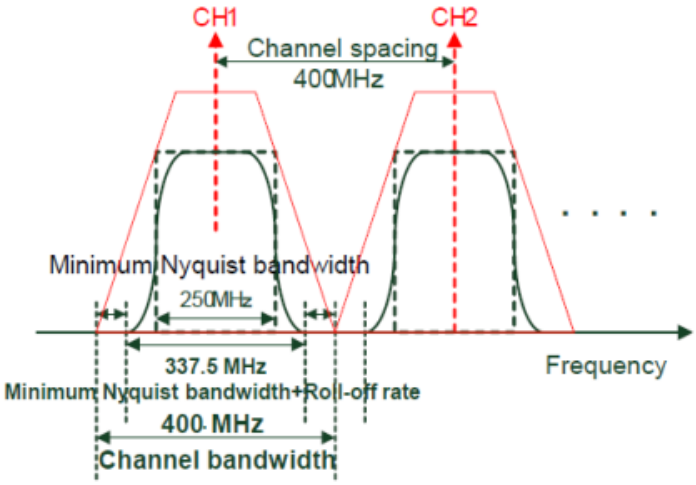

FIGURE 4

Measured characteristics of 44-dBi antenna

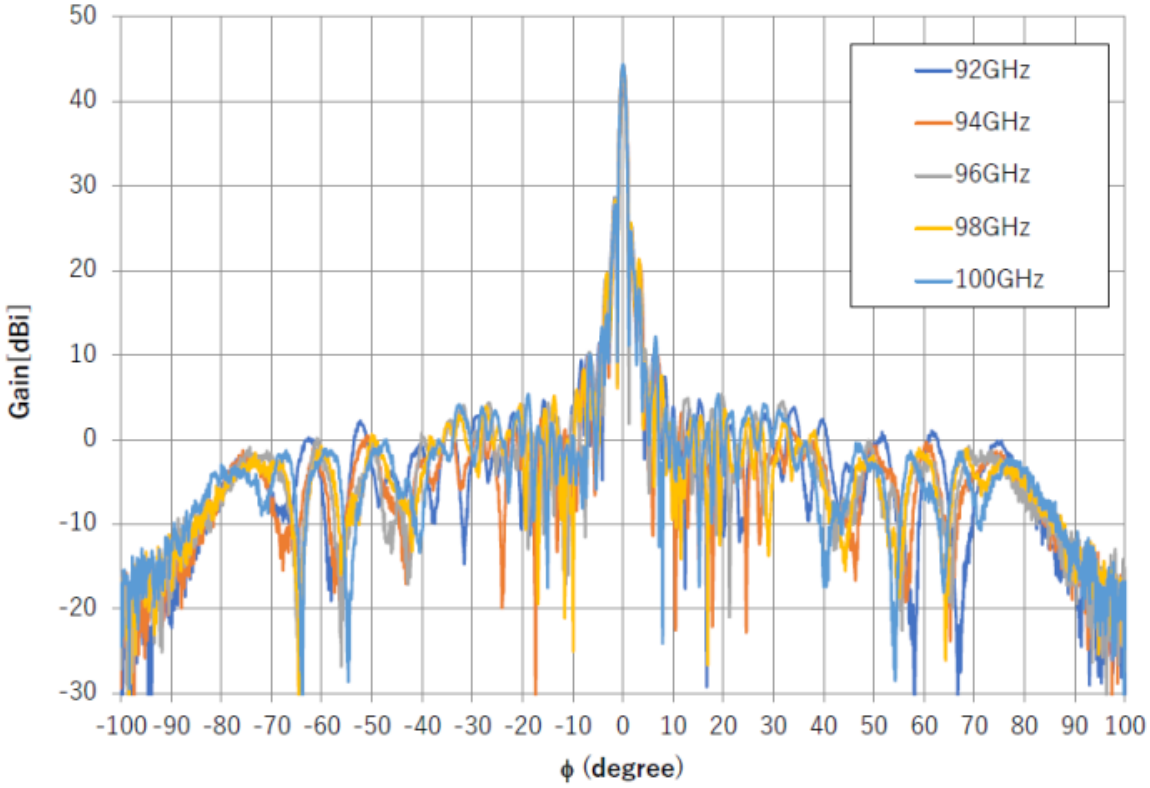

Railway RSTT stations are proposed to operate in the 92-94 GHz and 94.1-100 GHz frequency bands. These frequency bands are adjacent to the 94.0-94.1 GHz band which is allocated to the EESS (active) where spaceborne cloud profile radar (CPR) operate. The maximum RSTT OOB emissions into the 94.0-94.1 GHz band will occur when the railway RSST 250 MHz bandwidth signal is positioned at the band edge of the adjacent EESS (active) band.

4.1.3 Interference from railway RSTT systems into EESS (active)

For assessing the potential for interference from the railway RSTT systems into EESS active systems, three different geometrical scenarios are considered. The first is coupling of the antenna main lobe of a nadir-looking EESS (active) satellite with the sidelobes of the railway RSTT system antenna. The second geometrical scenario is coupling of the sidelobes of both the EESS active sensor antenna and the railway RSTT system antenna; and the third geometrical scenario is coupling between the mainbeam of the railway RSTT system antenna and the EESS active sensor antenna sidelobes occurring when the EESS active satellite is on the horizon with respect to the railway RSTT system.

The peak interfering signal power level, I (dBW), received by a spaceborne radar from a terrestrial source is calculated from

$$I = 10 \log P_t + G_t + G_r - (32.44 + 20 \log (f R)) - L_a \quad (1)$$

where:

P_t: peak terrestrial source transmitter power (W);

G_t: terrestrial source antenna gain towards spaceborne sensor (dBi);

G_r: spaceborne radar antenna gain towards terrestrial source (dBi);

f: frequency (MHz);

R: slant range between spaceborne sensor and terrestrial source (km);

L_a: attenuation due to atmospheric absorption (dB).

Attenuation due to atmospheric absorption, L_a, is dependent upon the path length to the satellite through the Earth's atmosphere, and hence upon the elevation angle from the terrestrial source to the satellite. At frequencies around 94 GHz, L_a decreases rapidly from about 100 dB at 0º elevation angles to 1.5 dB at 90º elevation angles. L_a is not included in the following tables of calculation of the interference levels and margins.

The interference due to mainlobe reception of the CPR antenna from the RSTT sidelobes allows for the highest values of RFI levels of the three geometrical scenarios. For CPR-L1 and CPR-L2, the CPR-L1 system is impacted the most by interference due to its narrower receiver bandwidth of 300 kHz. For geometric scenario 1 for coupling between the CPR-L1 mainlobe and the railway RSTT sidelobes (elevation angle at 90 º), preliminary calculations are provided in Tables 3 (Case 1) and 4 (Case 2) which indicate the amount of attenuation in regards to the in-band power emission level of the railway RSTT system needed to be applied to railway RSTT systems OOB emissions in order for them to meet the EESS (active) interference protection criteria. Considering CPR-L1, two cases were analyzed where the railway RSTT antenna gain in the sidelobes was –10 dBi and 14 dBi, and the density of railway RSTT systems was 10 and 100 in the CPR footprint. The EESS active noise figure used is 7 dB which results in the interference protection criteria threshold of -153.2 dBW. The calculated attenuations in regards to the in-band power emission level of the railway RSTT system needed to meet the EESS (active) interference protection criteria are 9.5 dB in Case 1 to 43.5 dB in Case 2.

For geometric scenario 2 for coupling between the CPR-L1 sidelobes and the railway RSTT sidelobes (elevation angle at 45º), preliminary calculations of two Cases examined are provided in Tables 5 (Case 1) and 6 (Case 2) which indicate the amount of attenuation in regards to the in-band power emission level of the railway RSTT system emissions in order that they meet the EESS (active) interference protection criteria for CPR-L1. The two cases were examined with the railway RSTT system antenna gain in the sidelobes at 0 dBi and 14 dBi, and the density of railway RSTT systems set at 10 and 100 in the CPR footprint, respectively. The EESS active system noise figure was 7 dB which resulted in the interference protection criteria threshold of -

153.2 dBW. The calculations show that the EESS (active) interference criteria are met with margins of 58.1 dB for Case 1 and 34.1 dB for Case 2.

For geometric scenario 3 for coupling between the CPR-L1 sidelobes and the railway RSTT mainlobe (elevation angle at 0º), preliminary calculations of two Cases examined are provided in Tables 7 (Case 1) and 8 (Case 2) which indicate the amount of attenuation in regards to the in-band power emission level of the railway RSTT system emissions in order that they meet the EESS (active) interference protection criteria for CPR-L1. The two cases were examined with the railway RSTT system antenna gain in the sidelobes at 44 dBi, and the density of railway RSTT systems set at 10 and 100 in the CPR footprint, respectively. The EESS active system noise figure was 7 dB which resulted in the interference protection criteria threshold of -153.2 dBW. The calculations show that the EESS (active) interference criteria are met with margins of 24.3 dB for Case 1 and 14.3 dB for Case 2.

TABLE 3

RFI from railway RSTT into EESS (active) at 94 GHz (Case 1)
First Geometric Scenario: CPR M/L to RSTT S/L

Case 1: Calculation of rcv pwr at 90 deg elev (G_t=-10 dBi, 10 railway RSTTs in beam)		
	CPR-L1	
	Value	**dB**
RSTT Transmit power,W	0.01	-20.00
Gain_xmit, dBi		-10.00
e.i.r.p., dBW		-30.00
Gain_rcv, dBi		65.20
$1/R^2$, km	705	-56.96
$1/f^2$, MHz	94050	-99.47
L-prop, dB		-188.87
No. of RSTTs in beam	10	10.00
Interf pwr, dBW		-143.67
k	1.38E-23	-228.60
Temp, K	290	24.62
BW_EESS, MHz	0.3	54.77
NF_EESS, dB		7.00
Noise pwr, dBW		-143.17
I/*N*, dB		-0.50
I/*N* criteria, dB		-10.00
Margin, dB (attenuation)		-9.50

TABLE 4

RFI from railway RSTT into EESS (active) at 94 GHz (Case 2)
First Geometric Scenario: CPR M/L to RSTT S/L

Case 2: Calculation of rcv pwr at 90 deg elev (G_t=14 dBi, 100 railway RSTTs in beam)		
	CPR-L1	
	Value	**dB**
Transmit power,W	0.01	-20.00
Gain_xmit, dBi		14.00
e.i.r.p., dBW		-6.00
Gain_rcv, dBi		65.20
$1/R^2$, km	705	-56.96
$1/f^2$, MHz	94050	-99.47
L-prop, dB		-188.87
No. of RSTTs in beam	100	20.00
Interf pwr, dBW		-109.67
k	1.38E-23	-228.60
Temp, K	290	24.62
BW_EESS, MHz	0.3	54.77
NF_EESS, dB		7.00
Noise pwr, dBW		-143.17
I/*N*, dB		33.50
I/*N* criteria, dB		-10.00
Margin, dB (attenuation)		-43.50

TABLE 5

RFI from railway RSTT into EESS (active) at 94 GHz (Case 1)
Second Geometric Scenario: CPR S/L to RSTT S/L

Case 1: Calculation of rcv pwr at 45 deg elev (G_t=0 dBi, 10 railway RSTTs in beam)		
	CPR-L1	
	Value	**dB**
RSTT Transmit power,W	0.01	-20.00
Gain_xmit, dBi		0.00
e.i.r.p., dBW		-20.00
Gain_rcv, dBi		-9.80
$1/R^2$, km	952	-59.57
$1/f^2$, MHz	94050	-99.47
L-prop, dB		-191.48
No. of RSTTs in beam	10	10.00
Interf pwr, dBW		-211.28
k	1.38E-23	-228.60
Temp, K	290	24.62
BW_EESS, MHz	0.3	54.77
NF_EESS, dB		7.00
Noise pwr, dBW		-143.17
I/*N*, dB		-68.11
I/*N* criteria, dB		-10.00
Margin, dB (attenuation)		58.11

TABLE 6

RFI from railway RSTT into EESS (active) at 94 GHz (Case 2)
Second Geometric Scenario: CPR S/L to RSTT S/L

Case 2: Calculation of rcv pwr at 45 deg elev (G_t=14 dBi, 100 railway RSTTs in beam)		
	CPR-L1	
	Value	**dB**
Transmit power,W	0.01	-20.00
Gain_xmit, dBi		14.00
e.i.r.p., dBW		-6.00
Gain_rcv, dBi		-9.80
$1/R^2$, km	952	-59.57
$1/f^2$, MHz	94050	-99.47
L-prop, dB		-191.48
No. of RSTTs in beam	100	20.00
Interf pwr, dBW		-187.28
k	1.38E-23	-228.60
Temp, K	290	24.62
BW_EESS, MHz	0.3	54.77
NF_EESS, dB		7.00
Noise pwr, dBW		-143.17
I/*N*, dB		-44.11
I/*N* criteria, dB		-10.00
Margin, dB (attenuation)		34.11

TABLE 7

RFI from railway RSTT into EESS (active) at 94 GHz (Case 1)
Third Geometric Scenario: CPR S/L to RSTT M/L

Case 1: Calculation of rcv pwr at 0 deg elev (G_t=44 dBi, 10 railway RSTTs in beam)		
	CPR-L1	
	Value	**dB**
RSTT Transmit power,W	0.01	-20.00
Gain_xmit, dBi		44.00
e.i.r.p., dBW		24.00
Gain_rcv, dBi		-9.80
$1/R^2$, km	3081	-69.77
$1/f^2$, MHz	94050	-99.47
L-prop, dB		-201.68
No. of RSTTs in beam	10	10.00
Interf pwr, dBW		-177.48
k	1.38E-23	-228.60
Temp, K	290	24.62
BW_EESS, MHz	0.3	54.77
NF_EESS, dB		7.00
Noise pwr, dBW		-143.17
I/*N*, dB		-34.31
I/*N* criteria, dB		-10.00
Margin, dB (attenuation)		24.31

TABLE 8

RFI from railway RSTT into EESS (active) at 94 GHz (Case 2)
Third Geometric Scenario: CPR S/L to RSTT M/L

Case 2: Calculation of rcv pwr at 0 deg elev (G_t=44 dBi, 100 railway RSTTs in beam)		
	CPR-L1	
	Value	**dB**
Transmit power,W	0.01	-20.00
Gain_xmit, dBi		44.00
e.i.r.p., dBW		24.00
Gain_rcv, dBi		-9.80
$1/R^2$, km	3081	-69.77
$1/f^2$, MHz	94050	-99.47
L-prop, dB		-201.68
No. of RSTTs in beam	100	20.00
Interf pwr, dBW		-167.48
k	1.38E-23	-228.60
Temp, K	290	24.62
BW_EESS, MHz	0.3	54.77
NF_EESS, dB		7.00
Noise pwr, dBW		-143.17
I/*N*, dB		-24.31
I/*N* criteria, dB		-10.00
Margin, dB (attenuation)		14.31

4.1.4 Interference from railway RSTT systems into EESS (passive)

For assessing the potential for interference from the railway RSTT systems into EESS passive systems, three different geometrical scenarios are considered. The first is coupling of the antenna main lobe of a conically scanning antenna of an EESS (passive) satellite with the sidelobes of the railway RSTT system antenna. The second geometrical scenario is coupling of the sidelobes of both the EESS passive sensor antenna and the railway RSTT system antenna; and the third geometrical scenario is coupling between the mainbeam of the railway RSTT system antenna and the EESS passive sensor antenna sidelobes occurring when the EESS passive satellite is on the horizon with respect to the railway RSTT system.

The peak interfering signal power level, *I* (dBW), received by a spaceborne radiometer from a terrestrial source is calculated from

$$I = 10 \log P_t + G_t + G_r - (32.44 + 20 \log (f R)) - L_a \quad (1)$$

where:

P_t : peak terrestrial source transmitter power (W);

G_t : terrestrial source antenna gain towards spaceborne sensor (dBi);

G_r : spaceborne radiometer antenna gain towards terrestrial source (dBi);

f : frequency (MHz);

R : slant range between spaceborne sensor and terrestrial source (km);

L_a : attenuation due to atmospheric absorption (dB).

Attenuation due to atmospheric absorption, L_a, is dependent upon the path length to the satellite through the Earth's atmosphere, and hence upon the elevation angle from the terrestrial source to the satellite. At frequencies around 92 GHz, L_a decreases rapidly from about 100 dB at 0º elevation angles to 1.5 dB at 90º elevation angles. L_a is not included in the following tables of calculation of the interference levels and margins.

The interference due to mainlobe reception of the radiometer L-8 antenna from the RSTT sidelobes allows for the highest values of RFI levels of the three geometrical scenarios. For geometric scenario 1 for coupling between the radiometer L-8 mainlobe and the railway RSTT sidelobes (elevation angle at 55 º), preliminary calculations are provided in Tables 9 (Case 1) and 10 (Case 2) which indicate the amount of attenuation in regards to the in-band power emission level of the railway RSTT system needed to be applied to railway RSTT systems OOB emissions in order for them to meet the EESS (passive) interference protection criteria. Considering radiometer L-8, two cases were analyzed where the railway RSTT antenna gain in the sidelobes was 0 dBi and 14 dBi, and the density of railway RSTT systems was 10 and 100 in the L-8 footprint. The EESS passive interference protection criteria threshold is -169.0 dBW. The calculated attenuations in regards to the in-band power emission level of the railway RSTT system needed to meet the EESS (passive) interference protection criteria are 18.7 dB in Case 1 to 52.7 dB in Case 2.

For geometric scenario 2 for coupling between the radiometer L-8 sidelobes and the railway RSTT sidelobes (elevation angle at 90º), preliminary calculations of two Cases examined are provided in Tables 11 (Case 1) and 12 (Case 2) which indicate the amount of attenuation in regards to the in-band power emission level of the railway RSTT system emissions in order that they meet the EESS (passive) interference protection criteria for radiometer L-8. The two cases were examined with the railway RSTT system antenna gain in the sidelobes at -10 dBi and 14 dBi, and the density of railway RSTT systems set at 10 and 100 in the L-8 footprint, respectively. The EESS passive interference protection criteria threshold is -169.0 dBW. The calculations show that the EESS (passive) interference criteria are met with margins of 49.4 dB for Case 1 and 15.4 dB for Case 2.

For geometric scenario 3 for coupling between the radiometer L-8 sidelobes and the railway RSTT mainlobe (elevation angle at 0º), preliminary calculations of two Cases examined are provided in Tables 13 (Case 1) and 14 (Case 2) which indicate the amount of attenuation in

regards to the in-band power emission level of the railway RSTT system emissions in order that they meet the EESS (passive) interference protection criteria for radiometer L-8. The two cases were examined with the railway RSTT system antenna gain in the sidelobes at 44 dBi, and the density of railway RSTT systems set at 10 and 100 in the L-8 footprint, respectively. The EESS passive interference protection criteria threshold is -169.0 dBW. The calculations show that the EESS (passive) interference criteria are met with margin of 8.3 dB for Case 1 but the calculated attenuation in regards to the in-band power emission level of the railway RSTT system needed to meet the EESS (passive) interference protection criteria is 1.7 dB for Case 2.

TABLE 9

RFI from railway RSTT into EESS (passive) at 92 GHz (Case 1)
First Geometric Scenario: L-8 M/L to RSTT S/L

Case 1: Calculation of rcv pwr at 55 deg elev (G_t=-10 dBi, 10 railway RSTTs in beam)		
	Radiometer L-8	
	Value	**dB**
RSTT Transmit power,W	0.01	-20.00
Gain_xmit, dBi		-10.00
e.i.r.p., dBW		-30.00
Gain_rcv, dBi		62.40
$1/R^2$, km	1 114.9	-60.94
$1/f^2$, MHz	92 000	-99.28
L-prop, dB		-192.66
No. of RSTTs in beam	10	10.00
Interf pwr, dBW		-150.26
Interf pwr criteria, dBW		-169.00
Margin, dB		-18.74

TABLE 10

RFI from railway RSTT into EESS (passive) at 92 GHz (Case 2)
First Geometric Scenario: L-8 M/L to RSTT S/L

Case 2: Calculation of rcv pwr at 55 deg elev (G_t=14dBi, 100 railway RSTTs in beam)		
	Radiometer L-8	
	Value	**dB**
Transmit power,W	0.01	-20.00
Gain_xmit, dBi		14.00
e.i.r.p., dBW		-6.00
Gain_rcv, dBi		62.40
$1/R^2$, km	1 114.9	-60.94
$1/f^2$, MHz	92 000	-99.28
L-prop, dB		-192.66
No. of RSTTs in beam	100	20.00
Interf pwr, dBW		-116.26
Interf pwr criteria, dBW		-169.00
Margin, dB		-52.74

TABLE 11

RFI from railway RSTT into EESS (passive) at 92 GHz (Case 1)
Second Geometric Scenario: L-8 S/L to RSTT S/L

Case 1: Calculation of rcv pwr at 90 deg elev (G_t=0 dBi, 10 railway RSTTs in beam)		
	Radiometer L-8	
	Value	**dB**
RSTT Transmit power,W	0.01	-20.00
Gain_xmit, dBi		-10.00
e.i.r.p., dBW		-30.00
Gain_rcv, dBi		-9.80
$1/R^2$, km	700	-56.90
$1/f^2$, MHz	92 000	-99.28

Case 1: Calculation of rcv pwr at 90 deg elev (G_t=0 dBi, 10 railway RSTTs in beam)		
	Radiometer L-8	
	Value	**dB**
L-prop, dB		-188.62
No. of RSTTs in beam	10	10.00
Interf pwr, dBW		-218.42
Interf pwr criteria, dBW		-169.00
Margin, dB		49.42

TABLE 12

RFI from railway RSTT into EESS (passive) at 92 GHz (Case 2)
Second Geometric Scenario: L-8 S/L to RSTT S/L

Case 2: Calculation of rcv pwr at 90 deg elev (G_t=14dBi, 100 railway RSTTs in beam)		
	Radiometer L-8	
	Value	**dB**
Transmit power,W	0.01	-20.00
Gain_xmit, dBi		14.00
e.i.r.p., dBW		-6.00
Gain_rcv, dBi		-9.80
$1/R^2$, km	700	-56.90
$1/f^2$, MHz	92 000	-99.28
L-prop, dB		-188.62
No. of RSTTs in beam	100	20.00
Interf pwr, dBW		-184.42
Interf pwr criteria, dBW		-169.00
Margin, dB		15.42

TABLE 13

RFI from railway RSTT into EESS (passive) at 92 GHz (Case 1)
Third Geometric Scenario: L-8 S/L to RSTT M/L

Case 1: Calculation of rcv pwr at 0 deg elev (G_t=44 dBi, 10 railway RSTTs in beam)		
	Radiometer L-8	
	Value	**dB**
RSTT Transmit power,W	0.01	-20.00
Gain_xmit, dBi		44.00
e.i.r.p., dBW		24.00
Gain_rcv, dBi		-9.80
$1/R^2$, km	3 069	-69.74
$1/f^2$, MHz	92 000	-99.28
L-prop, dB		-201.46
No. of RSTTs in beam	10	10.00
Interf pwr, dBW		-177.26
Interf pwr criteria, dBW		-169.00
Margin, dB		8.26

TABLE 14

RFI from railway RSTT into EESS (passive) at 92 GHz (Case 2)
Third Geometric Scenario: L-8 S/L to RSTT M/L

Case 2: Calculation of rcv pwr at 0 deg elev (G_t=44dBi, 100 railway RSTTs in beam)		
	Radiometer L-8	
	Value	**dB**
Transmit power,W	0.01	-20.00
Gain_xmit, dBi		44.00
e.i.r.p., dBW		24.00
Gain_rcv, dBi		-9.80
$1/R^2$, km	3 069	-69.74
$1/f^2$, MHz	92 000	-99.28

Case 2: Calculation of rcv pwr at 0 deg elev (G_t=44dBi, 100 railway RSTTs in beam)		
	Radiometer L-8	
	Value	dB
L-prop, dB		-201.46
No. of RSTTs in beam	100	20.00
Interf pwr, dBW		-167.26
Interf pwr criteria, dBW		-169.00
Margin, dB		-1.74

4.1.5 Preliminary Conclusions of Interference from railway RSTT systems into EESS (active) and EESS (passive)

For the EESS (active), the three different geometrical interaction scenarios described involving antenna beam coupling between railway RSTT systems and CPRs, the RFI levels at the CPR are highest for the geometrical situation of coupling between the nadir-looking CPR antenna and the sidelobes of the railway RSTT system antenna. With the second geometrical scenario where there is coupling of the sidelobes of both the CPR antenna and the railway RSTT system antenna; the RFI levels are lower than for the first geometric scenario. In the third geometrical scenario where coupling between the mainbeam of the railway RSTT system antenna and the CPR antenna sidelobes with the CPR satellite on the horizon with respect to the railway RSTT systems occurs, the interference was lower than the first geometric scenario as well. The CPR-L1 with the narrower receiver bandwidth of 300 kHz, is more sensitive than is CPR-L2. Two cases of railway RSTT deployment and their interference impact to CPR-L1 were analysed to arrive at a preliminary calculation of attenuation in regards to in-band emission levels of railway RSTT systems required to meet the Rec. ITU-R RS.1166-4 protection criteria for CPR-L1. The two cases consider the railway RSTT antenna gain in the sidelobes at the level in Figure 2 for the appropriate elevation angle and a higher level estimated due to irregularities in the trainside area, and the density of railway RSTT systems at 10 and 100 in the footprint of the CPR-L1 sensor. For the first geometric scenario, in order to meet the EESS (active) Rec. ITU-R RS.1166-4 protection criteria for CPR-L1, railway RSTT system in-band emission levels would have to be attenuated 9.5 dB when considering Case 1 and 43.5 dB when considering Case 2 at the band edges adjoining the EESS (active) band 94.0-94.1 GHz.

For the three different geometrical interaction scenarios described involving antenna beam coupling between railway RSTT systems and spaceborne radiometers, the RFI levels at the radiometer L-8 are highest for the geometrical situation of coupling between the mainlobe of the radiometer L-8 antenna and the sidelobes of the railway RSTT system antenna. With the second geometrical scenario where there is coupling of the sidelobes of both the radiometer L-8 antenna and the railway RSTT system antenna; the RFI levels are lower than for the first geometric

scenario. In the third geometrical scenario where coupling between the mainbeam of the railway RSTT system antenna and the radiometer L-8 antenna sidelobes with the radiometer L-8 satellite on the horizon with respect to the railway RSTT systems occurs, the interference was lower than the first geometric scenario as well. Two cases of railway RSTT deployment and their interference impact to radiometer L-8 were analysed to arrive at a preliminary calculation of attenuation in regards to in-band emission levels of railway RSTT systems required to meet the Rec. ITU-R RS.2017 protection criteria for L-8. The two cases consider the railway RSTT antenna gain in the sidelobes at the level in Figure 2 for the appropriate elevation angle and a higher level estimated due to irregularities in the trainside area, and the density of railway RSTT systems at 10 and 100 in the footprint of the L-8 sensor. For the first geometric scenario, in order to meet the EESS (passive) Rec. ITU-R RS.2017 protection criteria for spaceborne radiometers, railway RSTT system in-band emission levels would have to be attenuated 18.7 dB when considering Case 1 and 52.7 dB when considering Case 2 at the band edges adjoining the EESS (passive) band 86.0-92.0 GHz.

4.2 Compatibility studies for FOD detection systems and (EESS) (active)

4.2.1 System overview of foreign object debris detection system operating in the frequency band 92-100 GHz

Figure 5 illustrates the concept of the foreign object debris (FOD) detection system for runways. To balance the radar performance improvement and the system cost reduction, the high-accuracy and high-stability frequency modulated continuous wave (FMCW) radar signals are generated and up-converted to optical signals at the control tower, and transmitted through the optical fibre to the multiple FOD units placed along the runway area.

FIGURE 5

Schematic illustration of foreign object debris detection system in runway at airport

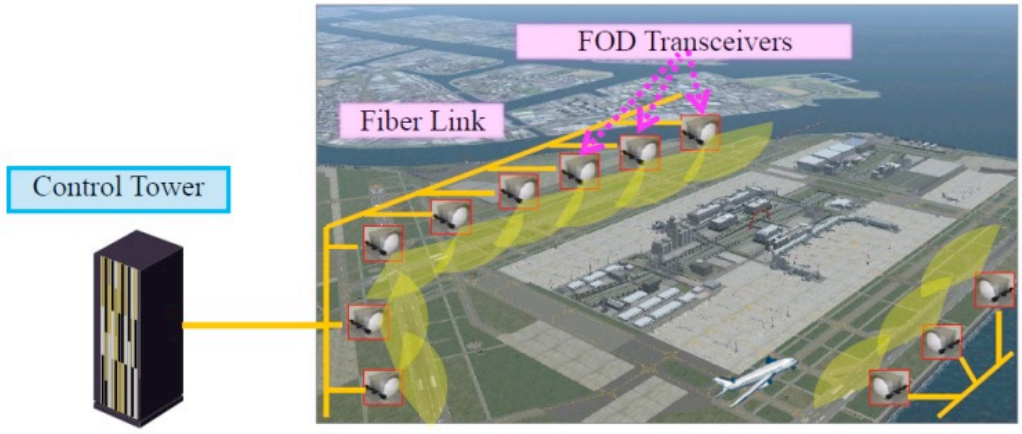

Figure 6 shows the overall configuration of FOD detection system including the control side equipment which is also named as the central processing unit. The equipment along the runway including the radar unit and the control side equipment (central processing unit) are connected through the optical fibre cables which are already installed in the runway area. The optical FMCW signals are generated by the laser source and electrical FMCW signals at the control side equipment, and are optically amplified and distributed via the optical divider to FOD units. The control side equipment receives the IF signals from each FOD unit and these intermediate frequency (IF) signals are processed by fast fourier transform (FFT) technology. FFT processing signals are displayed and stored as integrated FOD information.

FIGURE 6

Block diagram of foreign object debris detection system

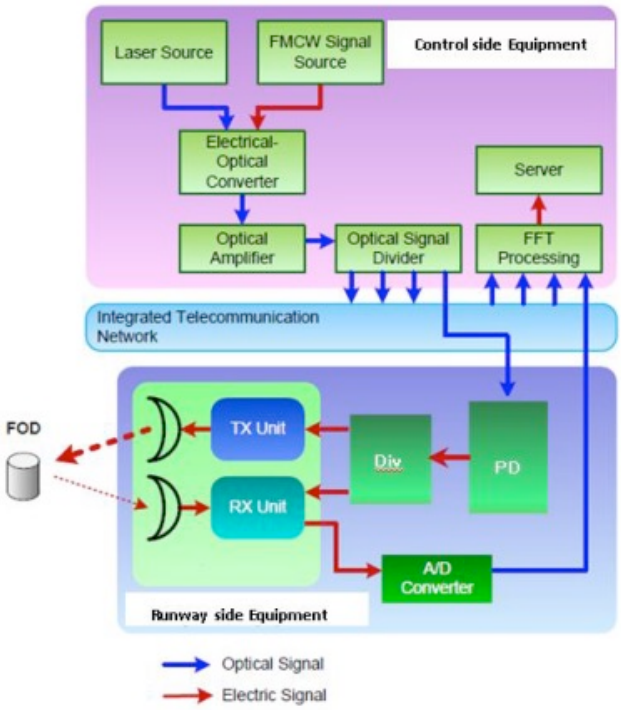

4.2.2 System characteristicx of foreign object debris detection system operating in the frequency band 92-100 GHz

Table 15 summarizes technical and operational characteristics of FOD detection systems operating in 92-100 GHz band.

Figure 7 shows the configuration of FOD unit which is connected through the radio over fibre technology to the central processing unit. To improve the receiving sensitivity, the Bi-Static type configuration is adopted. The optical FMCW signal whose subcarrier frequency is 30 GHz from the central processing unit is converted to the electrical FMCW signal by photo detector (PD), and the 30-GHz FMCW signal is amplified, tripled, again amplified and then radiated to the air. The radiated FMCW signal from Tx unit is reflected if the target object is on the runway and RX unit finally receives reflection signal. The received signal is down converted to the IF signal by the 90-GHz FMCW signal from the processing unit, and the IF signal is converted to digital signal by the A/D converter and transmitted to the central processing unit and to process information on locations of the target objects. The output spectrum of FOD unit is shown in Figure 8. Figure 9 shows the antenna gain pattern of the 44 dBi gain antenna.

TABLE 15

Technical and operational characteristics of foreign object debris detection system operating in the frequency band 92-100 GHz

Parameters	Units	Values
Frequency band	GHz	92-100
Output power	mW	200
Spectrum mask		See Figure 4
Sweep frequency	kHz or MHz	1 250
Antenna		Cassegrain
Full width at half maximum	degrees	Elevation:1.0, Azimuth: 1.0
Antenna rotation speed	rpm	15
Detection distance	m	500
Antenna elevation angle	degrees	-1.8 (see Figure 5)
Radiated rotation angle	degrees	±60
Radar cross section	dBsm*	-20
Range resolution	cm	5

* dBsm = decibels per square metre

FIGURE 7

Block diagram of foreign object debris transceiver

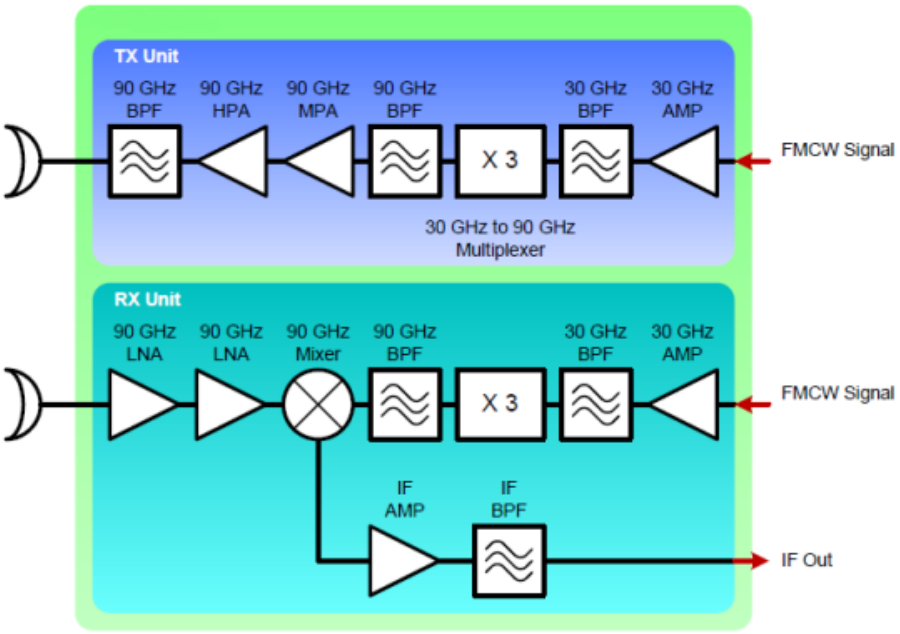

FIGURE 8

Spectrum mask of FOD detection system

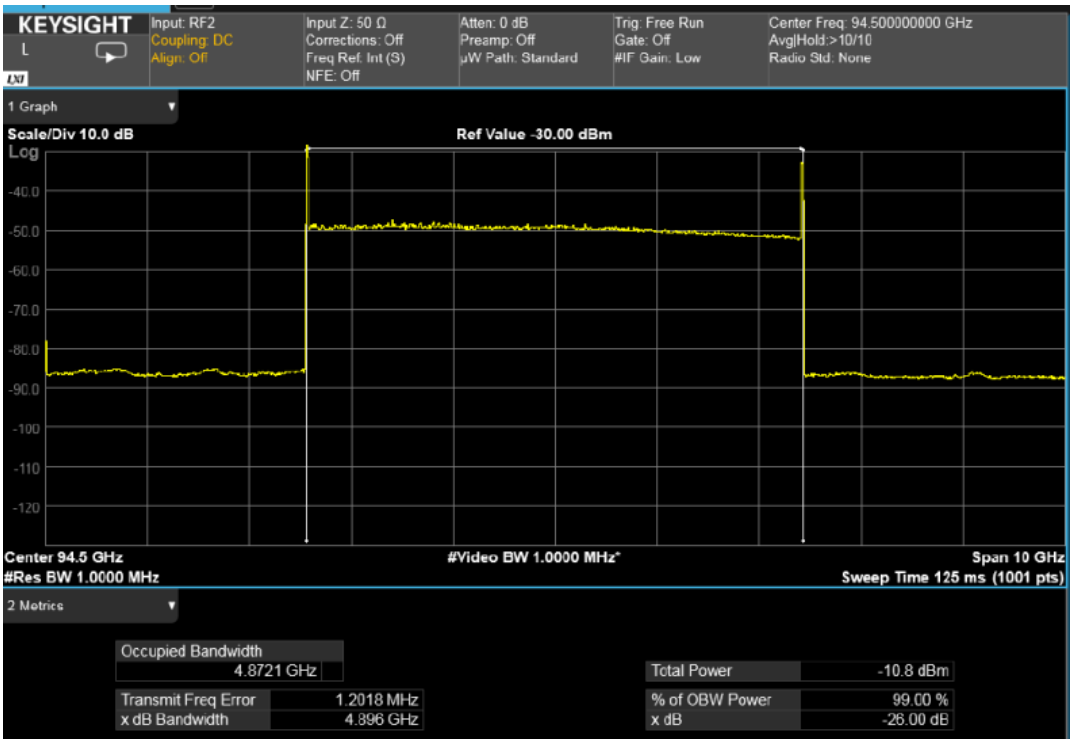

FIGURE 9

Measured characteristics of 44-dBi antenna

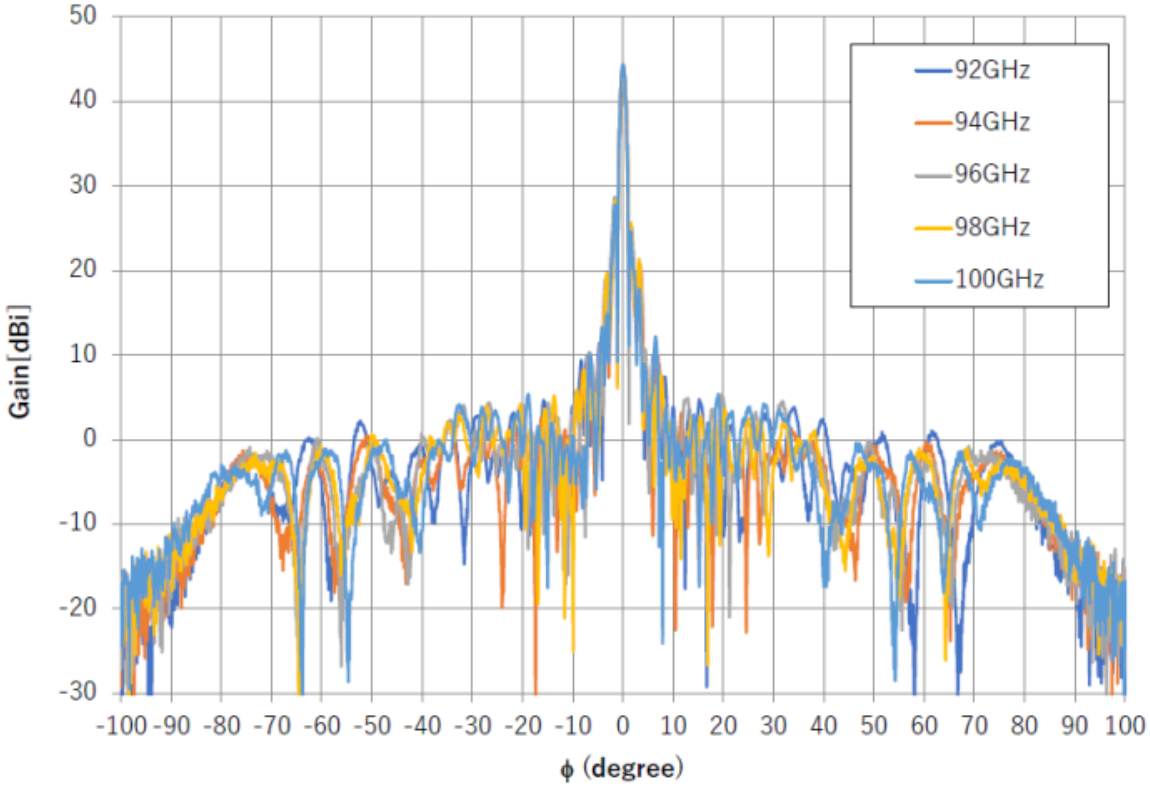

4.2.3 Interference from FOD detection systems into EESS (active)

At least three different geometrical scenarios have to be considered in assessing the potential for interference from FOD detection systems into EESS active systems. The first is coupling of the antenna mainlobe of a nadir-looking EESS (active) satellite with the sidelobes of the FOD detection system antenna. The second geometrical scenario is when coupling occurs between the sidelobes of both the EESS active sensor antenna and the FOD detection system antenna; and the third geometrical scenario is when coupling occurs between the mainbeam of the FOD detection system antenna and the EESS active sensor antenna sidelobes at a time when the EESS active satellite is on the horizon with respect to the FOD detection system.

The peak interfering signal power level, I (dBW), received by a spaceborne radar from a terrestrial source is calculated from

$$I = 10 \log P_t + G_t + G_r - (32.44 + 20 \log (f R)) - L_a \qquad (1)$$

where:

P_t : peak terrestrial source transmitter power (W);

G_t : terrestrial source antenna gain towards spaceborne sensor (dBi);

G_r : spaceborne radar antenna gain towards terrestrial source (dBi);

f : frequency (MHz);

R : slant range between spaceborne sensor and terrestrial source (km);

L_a : attenuation due to atmospheric absorption (dB).

Attenuation due to atmospheric absorption, L_a, is dependent upon the path length to the satellite through the Earth's atmosphere, and hence upon the elevation angle from the terrestrial source to the satellite. At frequencies around 94 GHz, L_a decreases rapidly from about 100 dB at 0º elevation angles to 1.5 dB at 90º elevation angles. L_a is not included in the following tables of calculation of the interference levels and margins.

The interference due to CPR antenna mainlobe coupling with the FOD detection system antenna sidelobes allows for the highest value of RFI levels of these three geometrical scenarios. For CPR L-1 and CPR L-2, the CPR L-1 system was found to be more sensitive to interference due to its narrower receiver bandwidth of 300 kHz. For geometric scenario 1 for coupling between the CPR L-1 mainlobe and the FOD sidelobes (elevation angle at 90º), preliminary calculations of two Cases examined are provided in Tables 16 (Case 1) and 17 (Case 2) which indicate the amount of attenuation needed to apply to in-band FOD detection systems emissions in order that they meet the EESS (active) interference protection criteria for CPR L-1. The two cases were examined with the FOD detection system antenna gain in the sidelobes at –10 dBi and 14 dBi, and the density of FOD detection systems set at 10 and 50 in the CPR footprint, respectively. The EESS active system noise figure was 7 dB which resulted in the interference protection criteria threshold of -153.2 dBW. The calculated attenuations needed to meet the EESS (active) interference criteria are 22.5 dB for Case 1 and 53.5 dB for Case 2.

For geometric scenario 2 for coupling between the CPR L-1 sidelobes and the FOD sidelobes (elevation angle at 45º), preliminary calculations of two Cases examined are provided in Tables 18 (Case 1) and 19 (Case 2) which indicate the amount of attenuation needed to apply to in-band FOD detection systems emissions in order that they meet the EESS (active) interference protection criteria for CPR L-1. The two cases were examined with the FOD detection system antenna gain in the sidelobes at 0 dBi and 14 dBi, and the density of FOD detection systems set at 10 and 50 in the CPR footprint, respectively. The EESS active system noise figure was 7 dB which resulted in the interference protection criteria threshold of -153.2 dBW. The calculations show that the EESS (active) interference criteria are met with margins of 45.1 dB for Case 1 and 24.1 dB for Case 2.

For geometric scenario 3 for coupling between the CPR L-1 sidelobes and the FOD mainlobe (elevation angle at 0º), preliminary calculations of two Cases examined are provided in Tables 20 (Case 1) and 21 (Case 2) which indicate the amount of attenuation needed to apply to in-band FOD detection systems emissions in order that they meet the EESS (active) interference protection criteria for CPR L-1. The two cases were examined with the FOD detection system antenna gain in the sidelobes at 44 dBi, and the density of FOD detection systems set at 10 and

50 in the CPR footprint, respectively. The EESS active system noise figure was 7 dB which resulted in the interference protection criteria threshold of -153.2 dBW. The calculations show that the EESS (active) interference criteria are met with margins of 11.3 dB for Case 1 and 4.3 dB for Case 2.

TABLE 16

RFI from FOD detection systems into EESS (active) at 94 GHz (Case 1)
First Geometric Scenario: CPR M/L to FOD S/L

Case 1: Calculation of rcv pwr at 90 deg elev (G_t=-10 dBi, 10 FODs in beam)		
	CPR-L1	
	Value	**dB**
Transmit power, W	0.2	-6.99
Gain_xmit, dBi		-10.00
e.i.r.p., dBW		-16.99
Gain_rcv, dBi		65.20
$1/R^2$, km	705	-56.96
$1/f^2$, MHz	94 050	-99.47
L-prop, dB		-188.87
No. of FODs in beam	10	10.00
Interf pwr, dBW		-130.66
k	1.38E-23	-228.60
Temp, K	290	24.62
BW_EESS, MHz	0.3	54.77
NF_EESS, dB		7.00
Noise pwr, dBW		-143.17
I/*N*, dB		12.51
I/*N* criteria, dB		-10.00
Margin, dB (attenuation)		-22.51

TABLE 17

RFI from FOD detection systems into EESS (active) at 94 GHz (Case 2)
First Geometric Scenario: CPR M/L to FOD S/L

Case 2: Calculation of rcv pwr at 90 deg elev (G_t=14dBi, 50 FODs in beam)		
	CPR-L1	
	Value	**dB**
Transmit power, W	0.2	-6.99
Gain_xmit, dBi		14.00
e.i.r.p., dBW		7.01
Gain_rcv, dBi		65.20
$1/R^2$, km	705	-56.96
$1/f^2$, MHz	94 050	-99.47
L-prop, dB		-188.87
No. of FODs in beam	50	16.99
Interf pwr, dBW		-99.67
k	1.38E-23	-228.60
Temp, K	290	24.62
BW_EESS, MHz	0.3	54.77
NF_EESS, dB		7.00
Noise pwr, dBW		-143.17
I/*N*, dB		43.50
I/*N* criteria, dB		-10.00
Margin, dB (attenuation)		-53.50

TABLE 18

RFI from FOD detection systems into EESS (active) at 94 GHz (Case 1)
Second Geometric Scenario: CPR S/L to FOD S/L

Case 1: Calculation of rcv pwr at 45 deg elev (G_t=0 dBi, 10 FODs in beam)		
	CPR-L1	
	Value	**dB**
Transmit power,W	0.2	-6.99
Gain_xmit , dBi		0.00
e.i.r.p., dBW		-6.99
Gain_rcv, dBi		-9.80
$1/R^2$, km	952	-59.57
$1/f^2$, MHz	94050	-99.47
L-prop, dB		-191.48
No. of FODs in beam	10	10.00
Interf pwr, dBW		-198.27
k	1.38E-23	-228.60
Temp, K	290	24.62
BW_EESS, MHz	0.3	54.77
NF_EESS, dB		7.00
Noise pwr, dBW		-143.17
I/*N*, dB		-55.10
I/*N* criteria, dB		-10.00
Margin, dB (attenuation)		45.10

TABLE 19

RFI from FOD detection systems into EESS (active) at 94 GHz (Case 2)
Second Geometric Scenario: CPR S/L to FOD S/L

Case 2: Calculation of rcv pwr at 45 deg elev (G_t=14dBi, 50 FODs in beam)		
	CPR-L1	
	Value	**dB**
Transmit power, W	0.2	-6.99
Gain_xmit, dBi		14.00
e.i.r.p., dBW		7.01
Gain_rcv, dBi		-9.80
$1/R^2$, km	952	-59.57
$1/f^2$, MHz	94050	-99.47
L-prop, dB		-191.48
No. of FODs in beam	50	16.99
Interf pwr, dBW		-177.28
k	1.38E-23	-228.60
Temp, K	290	24.62
BW_EESS, MHz	0.3	54.77
NF_EESS, dB		7.00
Noise pwr, dBW		-143.17
I/*N*, dB		-34.11
I/*N* criteria, dB		-10.00
Margin, dB (attenuation)		24.11

TABLE 20

RFI from FOD detection systems into EESS (active) at 94 GHz (Case 1)
Third Geometric Scenario: CPR S/L to FOD M/L

Case 1: Calculation of rcv pwr at 0 deg elev (G_t=44dBi, 10 FODs in beam)		
	CPR-L1	
	Value	**dB**
Transmit power, W	0.2	-6.99
Gain_xmit, dBi		44.00
e.i.r.p., dBW		37.01
Gain_rcv, dBi		-9.80
$1/R^2$, km	3081	-69.77
$1/f^2$, MHz	94050	-99.47
L-prop, dB		-201.68
No. of FODs in beam	10	10.00
Interf pwr, dBW		-164.47
k	1.38E-23	-228.60
Temp, K	290	24.62
BW_EESS, MHz	0.3	54.77
NF_EESS, dB		7.00
Noise pwr, dBW		-143.17
I/*N*, dB		-21.30
I/*N* criteria, dB		-10.00
Margin, dB (attenuation)		11.30

TABLE 21

RFI from FOD detection systems into EESS (active) at 94 GHz (Case 2)
Third Geometric Scenario: CPR S/L to FOD M/L

Case 2: Calculation of rcv pwr at 0 deg elev (G_t=44dBi, 50 FODs in beam)		
	CPR-L1	
	Value	**dB**
Transmit power, W	0.2	-6.99
Gain_xmit, dBi		44.00
e.i.r.p., dBW		37.01
Gain_rcv, dBi		-9.80
$1/R^2$, km	3081	-69.77
$1/f^2$, MHz	94050	-99.47
L-prop, dB		-201.68
No. of FODs in beam	50	16.99
Interf pwr, dBW		-157.48
k	1.38E-23	-228.60
Temp, K	290	24.62
BW_EESS, MHz	0.3	54.77
NF_EESS, dB		7.00
Noise pwr, dBW		-143.17
I/*N*, dB		-14.31
I/*N* criteria, dB		-10.00
Margin, dB (attenuation)		4.31

4.2.4 Interference from FOD detection systems into EESS (passive)

At least three different geometrical scenarios have to be considered in assessing the potential for interference from FOD detection systems into EESS passive systems. The first is coupling of the antenna mainlobe of a nadir-looking EESS (passive) satellite with the sidelobes of the FOD detection system antenna. The second geometrical scenario is when coupling occurs between the sidelobes of both the EESS passive sensor antenna and the FOD detection system antenna; and the third geometrical scenario is when coupling occurs between the mainbeam of the FOD detection system antenna and the EESS passive sensor antenna sidelobes at a time when the EESS passive satellite is on the horizon with respect to the FOD detection system.

The peak interfering signal power level, I (dBW), received by a spaceborne radiometer from a terrestrial source is calculated from:

$$I = 10 \log P_t + G_t + G_r - (32.44 + 20 \log (f R)) - L_a \quad (6)$$

where:

P_t : peak terrestrial source transmitter power (W);

G_t : terrestrial source antenna gain towards spaceborne sensor (dBi);

G_r : spaceborne radar antenna gain towards terrestrial source (dBi);

f : frequency (MHz);

R : slant range between spaceborne sensor and terrestrial source (km);

L_a : attenuation due to atmospheric absorption (dB).

Attenuation due to atmospheric absorption, L_a, is dependent upon the path length to the satellite through the Earth's atmosphere, and hence upon the elevation angle from the terrestrial source to the satellite. At frequencies around 94 GHz, L_a decreases rapidly from about 100 dB at 0º elevation angles to 1.5 dB at 90º elevation angles. L_a is not included in the following tables of calculation of the interference levels and margins.

The interference due to spaceborne antenna mainlobe coupling with the FOD detection system antenna sidelobes allows for the highest value of RFI levels of these three geometrical scenarios. For geometric scenario 1 for coupling between the radiometer L-8 mainlobe and the FOD sidelobes (elevation angle at 55º), preliminary calculations of two Cases examined are provided in Tables 22 (Case 1) and 23 (Case 2) which indicate the amount of attenuation needed to apply to OOB FOD detection systems emissions in order that they meet the EESS (passive) interference protection criteria for radiometer L-8. The two cases were examined with the FOD detection system antenna gain in the sidelobes at –10 dBi and 14 dBi, and the density of FOD detection systems set at 10 and 50 in the radiometer L-8 footprint, respectively. The EESS passive system interference protection criteria threshold is -169.0 dBW. The calculated attenuations needed to meet the EESS (passive) interference criteria are 31.75 dB for Case 1 and 62.74 dB for Case 2.

For geometric scenario 2 for coupling between the radiometer L-8 sidelobes and the FOD sidelobes (elevation angle at 90º), preliminary calculations of two Cases examined are provided in Tables 24 (Case 1) and 25 (Case 2) which indicate the amount of attenuation needed to apply to in-band FOD detection systems emissions in order that they meet the EESS (passive) interference protection criteria for radiometer L-8. The two cases were examined with the FOD detection system antenna gain in the sidelobes at 0 dBi and 14 dBi, and the density of FOD detection systems set at 10 and 50 in the radiometer L-8 footprint, respectively. The EESS passive system interference protection criteria threshold is -169.0 dBW. The calculations show that the EESS (passive) interference criteria are met with margins of 36.41 dB for Case 1 and 5.42 dB for Case 2.

For geometric scenario 3 for coupling between the radiometer L-8 sidelobes and the FOD mainlobe (elevation angle at 0º), preliminary calculations of two Cases examined are provided in Tables 26 (Case 1) and 27 (Case 2) which indicate the amount of attenuation needed to apply to in-band FOD detection systems emissions in order that they meet the EESS (passive)

interference protection criteria for radiometer L-8. The two cases were examined with the FOD detection system antenna gain in the sidelobes at 44 dBi, and the density of FOD detection systems set at 10 and 50 in the L-8 footprint, respectively. The EESS passive system interference protection criteria threshold is
-169.0 dBW. The calculated attenuations needed to meet the EESS (passive) interference criteria are 4.75 dB for Case 1 and 11.74 dB for Case 2.

TABLE 22

RFI from FOD detection systems into EESS (passive) at 92 GHz (Case 1)
First Geometric Scenario: L-8 M/L to FOD S/L

Case 1: Calculation of rcv power at 55 degrees elevation (G_t=-10 dBi, 10 FODs in beam)			
	Units	**Radiometer L-8**	
		Value	**dB**
Transmit power	W	0.2	-6.99
Gain transmit antenna	dBi		-10.00
e.i.r.p	dBW		-16.99
Gain receive antenna	dBi		62.40
$1/R^2$	km	1 114.9	-60.94
$1/f^2$	MHz	92 000	-99.28
L-prop	dB		-192.66
No. of FODs in beam		10	10.00
Interference power	dBW		-137.25
Interference power criteria	dBW		-169.00
Margin	dB		-31.75

TABLE 23

RFI from FOD detection systems into EESS (passive) at 92 GHz (Case 2)
First Geometric Scenario: L-8 M/L to FOD S/L

Case 2: Calculation of rcv power at 55 degrees elevation (G_t=14 dBi, 50 FODs in beam)			
	Units	**CPR-L1**	
		Value	**dB**
Transmit power	W	0.2	-6.99
Gain transmit antenna	dBi		14.00
e.i.r.p	dBW		7.01
Gain receive antenna	dBi		62.40
$1/R^2$	km	1 114.9	-60.94
$1/f^2$	MHz	92 000	-99.28
L-prop	dB		-192.66
No. of FODs in beam		50	16.99
Interference power	dBW		-106.26
Interference power criteria	dBW		-169.00
Margin	dB		-62.74

TABLE 24

RFI from FOD detection systems into EESS (passive) at 92 GHz (Case 1)
Second Geometric Scenario: L-8 S/L to FOD S/L

Case 1: Calculation of rcv power at 90 degrees elevation (G_t=0 dBi, 10 FODs in beam)			
	Units	**CPR-L1**	
		Value	**dB**
Transmit power	W	0.2	-6.99
Gain transmit antenna	dBi		-10.00
e.i.r.p	dBW		-16.99
Gain receive antenna	dBi		-9.80
$1/R^2$	km	700	-56.90
$1/f^2$	MHz	92 000	-99.28

Case 1: Calculation of rcv power at 90 degrees elevation (G_t=0 dBi, 10 FODs in beam)			
	Units	**CPR-L1**	
		Value	**dB**
L-prop	dB		-188.62
No. of FODs in beam		10	10.00
Interference power	dBW		-205.41
Interference power criteria	dBW		-169.00
Margin	dB		36.41

TABLE 25

RFI from FOD detection systems into EESS (passive) at 92 GHz (Case 2)
Second Geometric Scenario: L-8 S/L to FOD S/L

Case 2: Calculation of rcv power at 90 degrees elevation (G_t=14 dBi, 50 FODs in beam)			
	Units	**CPR-L1**	
		Value	**dB**
Transmit power	W	0.2	-6.99
Gain transmit antenna	dBi		14.00
e.i.r.p	dBW		7.01
Gain receive antenna	dBi		-9.80
$1/R^2$	km	700	-56.90
$1/f^2$	MHz	92 000	-99.28
L-prop	dB		-188.62
No. of FODs in beam		50	16.99
Interference power	dBW		-174.42
Interference power criteria	dBW		-169.00
Margin	dB		5.42

TABLE 26

RFI from FOD detection systems into EESS (passive) at 94 GHz (Case 1)
Third Geometric Scenario: L-8 S/L to FOD M/L

Case 1: Calculation of rcv power at 0 degrees elevation (G_t=44 dBi, 10 FODs in beam)			
	Units	**CPR-L1**	
		Value	**dB**
Transmit power	W	0.2	-6.99
Gain transmit antenna	dBi		44.00
e.i.r.p	dBW		37.01
Gain receive antenna	dBi		-9.80
$1/R^2$	km	3 069	-69.74
$1/f^2$	MHz	92 000	-99.28
L-prop	dB		-201.46
No. of FODs in beam		10	10.00
Interference power	dBW		-164.25
Interference power criteria	dBW		-169.00
Margin	dB		-4.75

TABLE 27

RFI from FOD detection systems into EESS (passive) at 92 GHz (Case 2)
Third Geometric Scenario: L-8 S/L to FOD M/L

Case 2: Calculation of rcv power at 0 degrees elevation (G_t=44 dBi, 50 FODs in beam)			
	Units	**CPR-L1**	
		Value	**dB**
Transmit power	W	0.2	-6.99
Gain transmit antenna	dBi		44.00
e.i.r.p	dBW		37.01
Gain receive antenna	dBi		-9.80
$1/R^2$	km	3 069	-69.74
$1/f^2$	MHz	92 000	-99.28
L-prop	dB		-201.46

Case 2: Calculation of rcv power at 0 degrees elevation (G_t=44 dBi, 50 FODs in beam)			
	Units	CPR-L1	
		Value	dB
No. of FODs in beam		50	16.99
Interference power	dBW		-157.26
Interference power criteria	dBW		-169.00
Margin	dB		-11.74

4.2.5 Preliminary conclusions on interference from FOD detection systems into EESS (active) and EESS (passive)

For EESS (active) systems, when initially considering three different geometrical interaction scenarios between FOD detection systems and CPR L-1, the RFI levels at the CPR are highest for the geometrical situation of coupling between the nadir-looking CPR antenna coupling and the sidelobes of the FOD detection system antenna. The RFI levels are lower than for this first scenario when considering the second geometrical scenario which examines coupling between the sidelobes of both the CPR antenna and the FOD detection system antenna. The third geometrical scenario is coupling between the mainbeam of the FOD detection system antenna and the CPR antenna sidelobes with the CPR satellite on the horizon with respect to the FOD detection system. The RFI levels in this third scenario are also lower than for the first scenario. The CPR L-1 with the narrower bandwidth of 300 kHz, is more sensitive to the impact of interference than is CPR L-2. Two cases of FOD detection system deployment and their interference impact to CPR L-1 were analysed to arrive at a preliminary calculation of attenuation of FOD detection system levels required to meet the Rec. ITU-R RS.1166-4 protection criteria for CPR L-1. The two cases consider the FOD detection system antenna gain in the sidelobes at the level in Figure 9 for the appropriate elevation angle and a slightly higher level estimated due to irregularities in the surrounding area, and the density of FOD detection systems at 10 and 50 in the footprint of the CPR L-1 sensor. For the first scenario, in order to meet the EESS (active) Rec. ITU-R RS.1166-4 protection criteria for CPR L-1, FOD detection system emissions would have to be attenuated 22.5 dB when considering Case 1 and 53.5 dB when considering Case 2.

For EESS (passive) systems, when initially considering three different geometrical interaction scenarios between FOD detection systems and radiometer L-8, the RFI levels at the radiometer L-8 are highest for the geometrical situation of coupling between the main-beam of the radiometer L-8 and the sidelobes of the FOD detection system antenna. The RFI levels are lower than for this first scenario when considering the second geometrical scenario which examines coupling between the sidelobes of both the radiometer L-8 antenna and the FOD detection system antenna. The third geometrical scenario is coupling between the main-beam of the FOD

detection system antenna and the radiometer L-8 antenna sidelobes with the radiometer L-8 satellite on the horizon with respect to the FOD detection system. The RFI levels in this third scenario are also lower than for the first scenario. Two cases of FOD detection system deployment and their interference impact to radiometer L-8 were analysed to arrive at a preliminary calculation of attenuation of FOD detection system levels required to meet the Rec. ITU-R RS.2017 protection criteria for radiometer L-8. The two cases consider the FOD detection system antenna gain in the sidelobes at the level in Figure 2 for the appropriate elevation angle and a slightly higher level estimated due to irregularities in the surrounding area, and the density of FOD detection systems at 10 and 50 in the footprint of the radiometer L-8 sensor. For the first scenario, in order to meet the EESS (passive) Rec. ITU-R RS.2017 protection criteria for radiometer L-8, FOD detection system emissions would have to be attenuated 31.8 dB when considering Case 1 and 62.7 dB when considering Case 2.